Chapter 3

Planar Waveguides

Optical signal transmission via fiberglass waveguides revolutionized telecommunication over long distances. The wavelength regimes around 1.3 μm and 1.55 μm are chosen because of extremely low absorption and dispersion windows for the silica fiberglass used. The loss requirements for planar waveguides on substrates with wafer-size (about 30 cm) to chip-size (about 1 cm) dimensions are less stringent. The wavelength window is open in the transparency regime, which is the near-infrared regime above 1.2 μm for silicon as the waveguide material. The application scenario and the availability of active devices define the upper limit. Now, germanium (Ge) on silicon (Si) active devices cover the wavelength range up to 1.55 μm. However, ongoing research with new semiconductor materials (strained Ge, GeSn, and low-bandgap III/V compounds) will extend the available range into the mid-infrared beyond 2.5 μm. Silicon, as the main material in the microelectronics industry, has attained great success; thus one wishes to utilize silicon as the base for photonic systems, too. The planar waveguide is an essential building block for photonic systems. So far, the silicon-on-insulator (SOI) platform has been the most popular structure for silicon waveguides. It has many advantages, such as high speed, low loss, small size, optoelectronic integration, and compatibility with the mature complementary metal-oxide semiconductor technology.

Silicon-Based Photonics
Erich Kasper and Jinzhong Yu

ISBN 978-981-4303-24-8 (Hardcover), 978-1-315-15651-4 (eBook)
www.jennystanford.com

Electromagnetic theory of light is the basis for understanding guided wave optics. Research on the effects of light in the waveguide, such as propagation, scattering, polarization, and diffraction, becomes the theoretical basis for a variety of waveguide devices. For silicon material, we want to study transmission, coupling, and interaction with the external field of light, especially the single-mode condition and transmission characteristic of the SOI waveguide. In the first part of the chapter, we will focus on the mode characteristics and single-mode conditions for the SOI waveguides, including the slab, strip, and rib waveguides, and then continue on the loss and polarization dependence in the SOI waveguide.

3.1 Modes in the Slab Waveguide

As a kind of electromagnetic wave, the propagation of light in a waveguide must satisfy Maxwell's equations. The material properties, structure, and dimensions of an optical waveguide are the boundary conditions for solving Maxwell's equations. To solve Maxwell's equations in the optical waveguide, we will get multiple different sets of eigenvalues and their corresponding eigenfunctions. The eigenfunction is the corresponding field distribution of the electromagnetic field components in the waveguide cross section, that is, it corresponds to the discrete mode of optical wave propagation. The eigenvalue is the propagation constant β of the corresponding mode in a given waveguide.

By solving Maxwell's equations, we first discuss the field distributions of various modes in the slab waveguide and then we extend them to the field distributions in strip and rib waveguides.

Maxwell's equations can be specifically expressed in the following forms (Eqs. 3.1–3.4):

$$\nabla \times \vec{E}(r,t) = -\frac{\partial \vec{B}(r,t)}{\partial t} \tag{3.1}$$

$$\nabla \times \vec{H}(r,t) = \vec{j} + \frac{\partial \vec{D}(r,t)}{\partial t} \tag{3.2}$$

$$\nabla \vec{D}(r,t) = \rho \tag{3.3}$$

$$\nabla \vec{B}(r,t) = 0 \tag{3.4}$$

Here, $\vec{j}$ is the vector of free current density, ρ is the volume density of free charge, ∇ is the Hamiltonian operator, $\vec{E}$ is the electric field vector, $\vec{H}$ is the magnetic field vector, $\vec{D}$ is the electric flux density or electric displacement vector, and $\vec{B}$ is the magnetic flux density vector. They are all related to the time variation t and the position vector r. For a passive dielectric medium, it has no current and charge sources, so $\rho = 0$ and $\vec{j} = 0$, and Maxwell's equations can be simplified.

In the classical theory, there are the constitutive relations between the flux densities $\vec{D}$ and $\vec{B}$ as well as the fields $\vec{E}$ and $\vec{H}$. For a linear and isotropic medium, the relations are given by

$$\vec{D} = \varepsilon\vec{E} \tag{3.5}$$

$$\vec{B} = \mu\vec{H} \tag{3.6}$$

where ε is the dielectric permittivity of the medium and μ is the magnetic permeability of the medium. For a linear dielectric medium, the permittivity ε and permeability μ are independent of field intensities, but most dielectric mediums become nonlinear when the electric field intensity is relatively high. For a lossless medium, ε and μ are real scalar; while for an absorbing medium, they are complex scalar. If we substitute the constitutive relations (Eqs. 3.5 and 3.6) into Maxwell's equations, assuming that the medium is homogeneous, we can derive the following basic wave equations for $\vec{E}$ and $\vec{H}$:

$$\nabla^2\vec{E} - \mu\varepsilon\frac{\partial^2\vec{E}}{\partial t^2} = 0 \tag{3.7}$$

$$\nabla^2\vec{H} - \mu\varepsilon\frac{\partial^2\vec{H}}{\partial t^2} = 0 \tag{3.8}$$

Generally, electromagnetic waves are related to time by a sinusoidal relationship. The electromagnetic wave is radiated with a single frequency or can even be decomposed into many single-frequency waves by using Fourier transforms. Hence, the electric field vector and magnetic field vector can be written in the following forms:

$$\vec{E}(r,t) = \vec{E}(r)\exp(-i\omega t) \tag{3.9}$$

$$\vec{H}(r,t) = \vec{H}(r)\exp(-i\omega t) \tag{3.10}$$

Here $\vec{E}(r)$ and $\vec{H}(r)$ are the complex amplitude vectors and ω is the angular frequency. Substituting Eqs. 3.9 and 3.10 into Maxwell's equations (Eqs. 3.1 and 3.2), we get

$$\nabla \times \vec{E}(r) = i\omega\mu_0 \vec{H}(r) \tag{3.11}$$

and

$$\nabla \times \vec{H}(r) = -i\omega\varepsilon_0 n^2 \vec{E}(r)\,, \tag{3.12}$$

where ε_0 and μ_0 are free space permittivity and free space permeability, respectively. For nonmagnetic dielectric mediums, $\mu = \mu_0$ and n is the refractive index of the medium and satisfies the relation $\varepsilon = \varepsilon_0 n^2$.

Now we solve Maxwell's equations in the planar dielectric waveguide, and then we can further analyze the electromagnetic wave modes in the waveguide. The slab waveguide is the simplest optical waveguide as shown in Fig. 3.1, and there are accurate analytical solutions to this waveguide. The slab waveguide consists of a guiding layer (or core layer), a substrate layer, and a cover layer or cladding layer. Their refractive indexes are n_1, n_2, and n_3, respectively, and commonly $n_1 > n_2 \geq n_3$. In the slab waveguide, the thickness of the core layer is d, which is much smaller than the waveguide width. So this waveguide can be considered infinite in the horizontal direction (y axis), namely

$$\frac{\partial \vec{E}}{\partial y} = \frac{\partial \vec{H}}{\partial y} = 0\,. \tag{3.13}$$

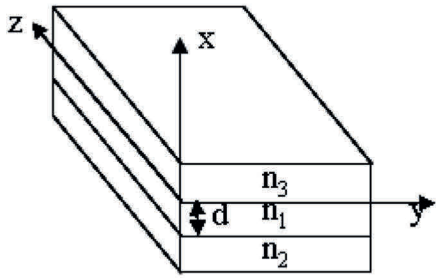

Figure 3.1 Planar dielectric waveguide.

Going by the coordinate axes shown in Fig. 3.1, the electric and magnetic fields are not functions of y for an electromagnetic wave propagating along the z axis. We assume the electric field polarizing along the y axis; the solutions to the wave equations should have the following forms:

$$E_y(x,z,t) = E(x)\exp[i(\beta z - \omega t)] \tag{3.14}$$

$$H_x(x,z,t) = H(x)\exp[i(\beta z - \omega t)] \tag{3.15}$$

If we substitute Eqs. 3.14 and 3.15 into Eqs. 3.11 and 3.12, we get the following:

$$\left.\begin{aligned} \beta E_y &= -\omega\mu H_x \\ \frac{\partial E_y}{\partial x} &= i\omega\mu H_z \\ i\beta H_x - \frac{\partial H_z}{\partial x} &= -i\omega\varepsilon E_y \end{aligned}\right\} \tag{3.16}$$

$$\left.\begin{aligned} \beta H_y &= \omega\varepsilon E_x \\ \frac{\partial H_y}{\partial x} &= -i\omega\varepsilon E_z \\ i\beta E_x - \frac{\partial E_z}{\partial x} &= i\omega\mu H_y \end{aligned}\right\} \tag{3.17}$$

As discussed in classical theory, there are two possible electromagnetic field polarizations, that is, the transverse electric (TE) field and the transverse magnetic (TM) field. The electric field of a TE wave exists only in the transverse direction, which means that there is no electric field component in the propagation direction; the magnetic field of a TM wave exists only in the transverse direction, which means that there is no magnetic field component in the propagation direction. Waves in a slab waveguide can be also classified as TE and TM waves. Looking at the above two sets of equations, these two sets of equations are independent of each other, and their solutions are also independent. There are only electromagnetic components E_y, H_x, and H_z in the Eqs. 3.16 and only electromagnetic components H_y, E_x, and E_z in Eqs. 3.17. Applying some assumptions, the solutions of these two sets of equations are a TE wave and a TM wave, respectively. If we consider one of the two waves, the TE wave, $E_z = 0$. Inserting it into Eqs. 3.17, we get

$$\partial H_y/\partial x = 0$$

that is, H_y is a constant independent of x. We assume this constant is zero because it doesn't have influence on the calculation results. From Eqs. 3.16, we know that E_x is zero too. Hence, the TE wave only has the electric field E_y component and the magnetic field H_x and H_z components. Similarly, inserting H_z = 0 into Eqs. 3.16, we can also obtain the TM wave with only the magnetic field H_y component and the electric field E_x and E_z components.

For simplification, Eqs. 3.16 and 3.17 can be reduced to the Helmholtz scalar equations of TE wave and TM wave, which are also called wave equations:

$$\frac{\partial^2 E_y}{\partial x^2} + (k_0^2 n_j^2 - \beta^2) E_y = 0 \tag{3.18}$$

$$\frac{\partial^2 H_y}{\partial x^2} + (k_0^2 n_j^2 - \beta^2) H_y = 0 \tag{3.19}$$

where $$k_0 = \omega\sqrt{\varepsilon_0 \mu_0} = 2\pi/\lambda .$$

The above equations are second-order differential equations, and they are solved by imposing the additional boundary conditions. The forms of the solutions to these second-order differential equations are related to the comparison of the magnitude between $k_0 n_j$ and β. If $k_0 n_j < \beta$, the solution is an oscillatory function (sinusoidal form); on the other hand, if $k_0 n_j > \beta$, the solution is an exponentially decaying function. On using the different propagation constant β to solve Eqs. 3.18 and 3.19, we can obtain different solutions with different field distribution in the slab waveguide. Each possible solution of β is called a mode. The modes in the slab waveguide can be classified as guided mode ($k_0 n_2 < \beta < k_0 n_1$), substrate mode ($k_0 n_3 < \beta \leq k_0 n_2$), and radiation mode ($0 \leq \beta \leq k_0 n_3$). For the guided mode, $k_0 n_2 < \beta < k_0 n_1$, solutions to the wave equation are exponentially decaying in the substrate layer and cladding layer; however, oscillatory waves form in the core layer. For the substrate mode, $k_0 n_3 < \beta \leq k_0 n_2$, solutions to the wave equation are exponentially decaying in the cladding layer, while oscillatory waves form in the substrate layer and the core layer. For the radiation mode, $0 \leq \beta \leq k_0 n_3$, there are oscillatory waves in all three layers of the waveguide. From the above discussion, we find that only when propagation constant β is in the range for the guided mode ($k_0 n_2 < \beta < k_0 n_1$), the electromagnetic wave can propagate in the guided layer. However, for the substrate mode, light waves will penetrate out of the waveguide through the substrate layer; for the radiation mode, light waves will penetrate out of the waveguide through the substrate layer and the cladding layer. Generally, it is deemed that the cladding and substrate layers have absorbing and scattering function for light waves, so light waves propagate in the two layers with a large loss and may even disappear. Therefore, we should avoid the latter two modes in the waveguide.

For simplicity, we take the TE wave as an example. To solve Eq. 3.18, according to the solution types in the guided mode case analyzed above, we can assume the electric field in the three layers of the slab waveguide to be written as follows:

$$E_y(x) = \begin{cases} A_1 \exp(-\delta x) & 0 \le x < +\infty \\ A\cos(\kappa x) + B\sin(\kappa x) & -d \le x \le 0 \\ A_2 \exp(\gamma x) & -\infty < x \le -d \end{cases}, \tag{3.20}$$

where A, B, A_1, and A_2 are amplitude coefficients to be determined by the boundary conditions, κ, γ, and δ, which are defined as follows:

$$\begin{aligned} \kappa &= (k_0^2 n_1^2 - \beta^2)^{1/2} \\ \gamma &= (\beta^2 - k_0^2 n_2^2)^{1/2} \\ \delta &= (\beta^2 - k_0^2 n_3^2)^{1/2} \end{aligned} \tag{3.21}$$

Considering the continuity of the electric field at $x = 0$ and $x = -d$, the boundary conditions are as follows:

$$\begin{cases} E_y(0^-) = E_y(0^+) \\ E_y(-d^-) = E_y(-d^+) \end{cases} \tag{3.22}$$

Combining Eq. 3.16 and boundary condition 3.22, we can get

$$\tan(\kappa d) = \frac{\kappa(\gamma + \delta)}{\kappa^2 - \gamma\delta} \tag{3.23}$$

Equation 3.23 is the characteristic equation for the TE modes of the slab waveguide. All the parameters (κ, γ, and δ) in the equation depend on the propagation constant β, so it is also the eigenvalue equation of β for TE modes of the slab waveguide. Because the equation is transcendental, the solutions for β to this equation need to be calculated numerically. We can consider κd as a variable. Using the mapping approach, we can get multiple sets of eigenvalue propagation constants and their corresponding field distributions, where each set of solutions corresponds to a propagation mode in the waveguide. Similarly, we can derive the characteristic equation for the TM modes of the slab waveguide:

$$\tan(\kappa d) = \frac{n_1^2 \kappa (n_2^2 \delta + n_3^2 \gamma)}{(n_2^2 n_3^2 \kappa^2 - n_1^4 \delta \gamma)} \tag{3.24}$$

Let us look at the solutions, Eqs. 3.20, in the slab waveguide again. The solution is sinusoidal in the core layer, which is a periodic function. Therefore, the possible value of β is discrete, that is, there are a limited number of modes that can exist in the slab waveguide.

From Eqs. 3.20 and 3.21 and the continuity of the field components in the x direction, comprehensively considering TE and TM modes, we can get

$$(n_1^2 - N^2)^{1/2} k_0 d = m\pi + \arctan\left(\sqrt{\frac{N^2 - n_2^2}{n_1^2 - N^2}}\eta_2\right) + \arctan\left(\sqrt{\frac{N^2 - n_3^2}{n_1^2 - N^2}}\eta_3\right), \tag{3.25}$$

where $N = \beta/k_0$ is the effective refractive index of the mode; for the TE mode, $\eta_{2,3} = 1$; for the TM mode, $\eta_{2,3} = (n_1/n_{2,3})^2$. From the process of derivation, we find that Eq. 3.25 is equivalent to the characteristic Eqs. 3.23 and 3.24 for the TE or TM modes of the slab waveguide. m is called the mode number, $m = 0, 1, 2, \ldots$, where each m corresponds to an effective refractive N, which also proves the above analysis that the possible value of β is discrete.

Considering the most popular silicon waveguide system, that is, the silicon-on-insulator (SOI) platform, the three layers of the slab waveguide, as shown in Fig. 3.1, are air, silicon, and silica, with the corresponding refractive indices n_3, n_1, and n_2. The thickness of the middle silicon guiding layer is d. From the above discussion, solving the Helmholtz equations, we can obtain the analytical solutions of the waveguide modes. Figure 3.2 shows the field distributions of a few low-order TE and TM modes when the thickness d = 1 μm. Figure 3.2 shows that the field distributions penetrate deeper into the cladding and substrate layers when the mode number m increases. From Eq. 3.25, we find that when the mode number m increases, the effective refractive index N decreases, that is, the propagation constant β decreases. When the waveguide thickness d increases, the propagation constant β increases, and when the thickness is greater, the waveguide can support more guided modes. Figure 3.3 shows the relationship between the propagation constant of the first eight guided modes (including both TE and TM modes) and the silicon layer thickness. Due to the guided mode condition ($k_0n_2 < \beta < k_0n_1$), the mode number m cannot be infinitely large. Only a finite number of modes will be guided in the waveguide. If the waveguide thickness reduces to below some value, the waveguide will support only one mode with a polarization (TE or TM), which is the so-called single-mode waveguide. To reduce the interaction between the high-order modes, we usually prefer single-mode waveguides.

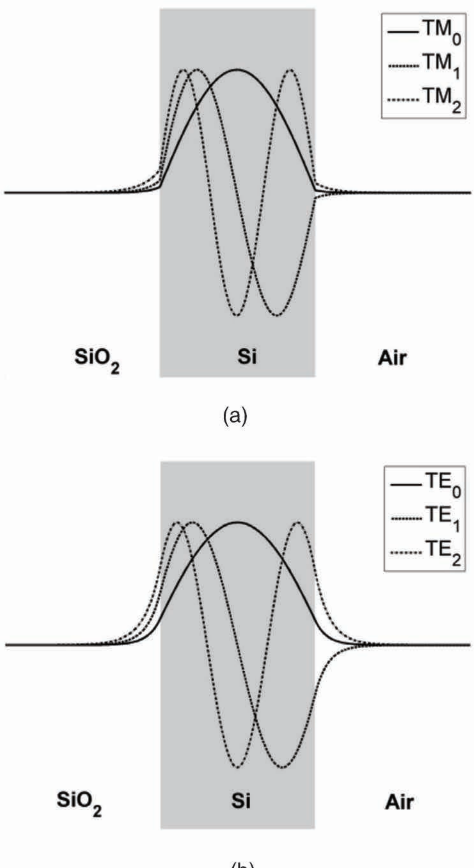

Figure 3.2 Field distributions for (a) TE_0, TE_1, and TE_2 modes and (b) TM_0, TM_1, TM_2 modes, when the silicon thickness d = 1 μm (1.55 μm wavelength).

If we take into consideration the guided mode condition $k_0 n_2 < \beta < k_0 n_1$, then $\beta = k_0 n_2$ is the cutoff condition of the slab waveguide guided modes. Therefore, we have the cutoff equation of guided modes

$$(n_1^2 - n_2^2)^{\frac{1}{2}} k_0 d = m\pi + \arctan\left(\sqrt{\frac{n_2^2 - n_3^2}{n_1^2 - n_2^2}}\eta_3\right). \tag{3.26}$$

From Eq. 3.26, we can also derive the condition of the slab waveguide maintaining single-mode operation as follows:

$$\begin{aligned}\frac{1}{k_0\sqrt{n_1^2 - n_2^2}}\arctan\left(\sqrt{\frac{n_2^2 - n_3^2}{n_1^2 - n_2^2}}\eta_3\right) < d < \frac{1}{k_0\sqrt{n_1^2 - n_2^2}} \\ \left[\pi + \arctan\left(\sqrt{\frac{n_2^2 - n_3^2}{n_1^2 - n_2^2}}\eta_3\right)\right],\end{aligned} \tag{3.27}$$

where $k_0 = \dfrac{2\pi}{\lambda}$ is the wave number of light waves in vacuum and λ is the wavelength. The left part of the above equation is the cutoff thickness for TE_0 and TM_0 modes, and the right part is the cutoff thickness for TE_1 and TM_1 modes. Substituting the real refractive index of air, silicon, and silica into Eq. 3.27, we can get the single-mode condition 26.27 nm < d < 274.58 nm for TE mode and 105.28 nm < d < 353.59 nm for TM mode (1.55 μm wavelength). Obviously, in order to achieve single-mode transmission in the air/silicon/silica three-layer dielectric slab waveguide, we must reduce its size to the order of submicrons.

The above discussion reveals the basic methods to analyze the modes in the waveguide. For the analysis of the multilayer slab waveguides, strip waveguide and rib waveguide, the differences in methods are because of the differences in boundary conditions. We can analyze them by considering that the effective index method (EIM) is equivalent to the multilayer slab waveguide. Solving the propagation constants of the modes and the corresponding field distributions is the fundamental approach to analyzing the modes in the waveguide. The related issues are treated in the classical literature [1]; so we will not review them here.

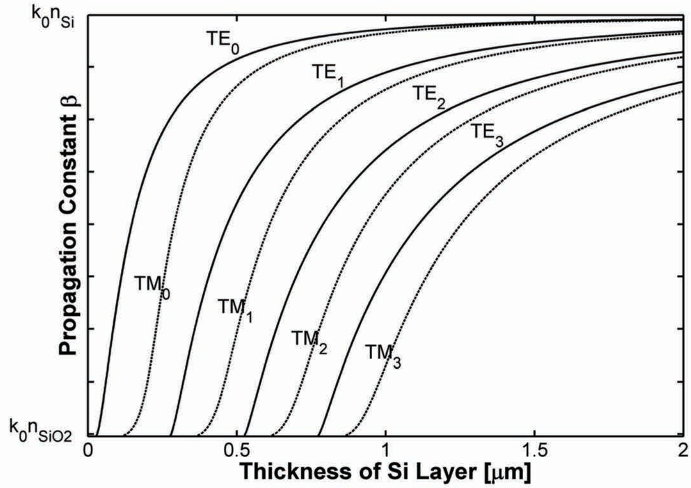

Figure 3.3 Relationship between the propagation constant β of the TE and TM modes and the silicon layer thickness (1.55 μm wavelength).

3.2 Strip Waveguides and Rib Waveguides

The slab waveguides confine light waves to only one dimension; the waveguide must be very thin to meet the single-mode condition. To confine light better, 2D confinement waveguides are required. There are two common basic SOI waveguide structures: strip waveguides (or photonic wires [2]) and rib waveguides, as shown in Fig. 3.4. The cross sections of the strip and rib waveguides can be rectangular (Fig. 3.4) or any other shape (such as a trapezoidal cross section). They confine light waves both in the horizontal and vertical directions, so an analytical solution of the modes in these waveguides cannot be directly obtained by mathematical derivation of the Helmholtz equations. When the widths of the strip and rib waveguides increase, the waveguide can support more guided modes, which is similar to the 1D slab waveguides. To analyze the modes in the waveguide, many approximate or numerical solutions have been developed, such as the EIM, the beam propagation method (BPM), the finite difference time domain, and the film mode–matching method.

To achieve single-mode operation, strip waveguide dimensions in both directions (height and width) should be below certain cutoff values. The SOI waveguide cutoff dimensions are usually smaller than 1 μm due to the high refractive index contrast between silicon (~3.5) and silica (~1.5). By using different numerical methods from the above description, one can accurately calculate the cutoff dimension of certain waveguide type and obtain the single-mode condition.

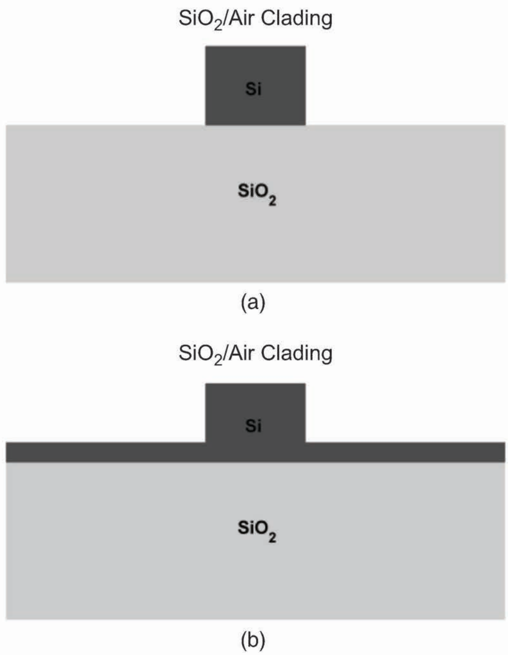

Figure 3.4 The cross-section structure diagram of (a) strip waveguides and (b) rib waveguides.

Figure 3.5 shows the single-mode condition for a strip waveguide with oxide cladding [3] when a full-vector finite difference method is used for calculation. The horizontal and vertical axes in Fig. 3.5 are the width *w* and height *h* of the core, respectively. The curves indicate the critical boundary under which the single-mode region lies. The size of the core for a single-mode Si strip waveguide is of the order of several hundred nanometers. Similar to 2D slab waveguides, the fundamental modes for TE and TM polarization in a 1D waveguide also have a cutoff condition. The single-mode region is located between the curves that are determined by the cutoff conditions for the fundamental and first-order modes. We have two curves for each TE and TM polarization in a width *w* versus height *H* presentation (Fig. 3.6), which define the single-mode region for both modes (black color) and adjacent regions in which either TE or TM is single mode.

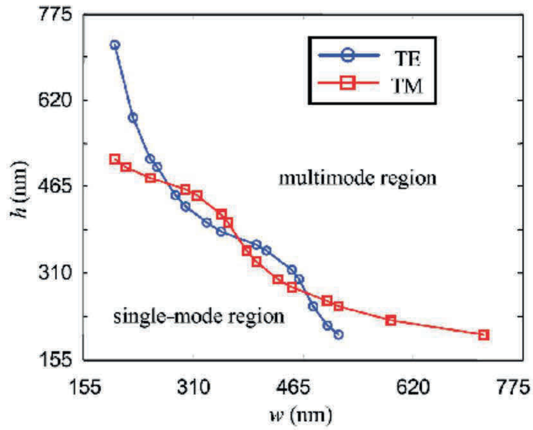

Figure 3.5 Single-mode conditions for the TE and TM modes of a strip waveguide with oxide cladding (1.55 µm wavelength). Reprinted with permission from Ref. [3] © The Optical Society.

Soon Lim et al. solved the cross-section field and effective refractive index of the strip waveguide by using a 3D imaginary BPM and analyzed the single-mode conditions [4] of the strip waveguide with oxide cladding at both operating wavelengths, 1310 nm and 1550 nm, in detail, as shown in Fig. 3.6. To satisfy single-mode conditions in both polarizations (TE and TM), two conditions have to be considered: (i) the cutoff condition of the first-order TE mode (upper limit) and (ii) the cutoff condition of the fundamental TM mode (lower limit). Let us consider a waveguide dimension of 300 nm × 350 nm; the result indicates that the waveguide is single mode at a wavelength of 1550 nm but not at a wavelength of 1310 nm; this implies that the single-mode condition is more relaxed at longer wavelengths and more stringent at shorter wavelengths. If the boundaries of the TM_0 and TE_1 cutoffs are fitted, we can obtain an experiential equation that describes the single-mode condition at wavelength 1550 nm as follows:

$$0.2+162e^{-H/0.03} \leq W \leq 0.3+5.9e^{-H/0.08} \tag{3.28}$$

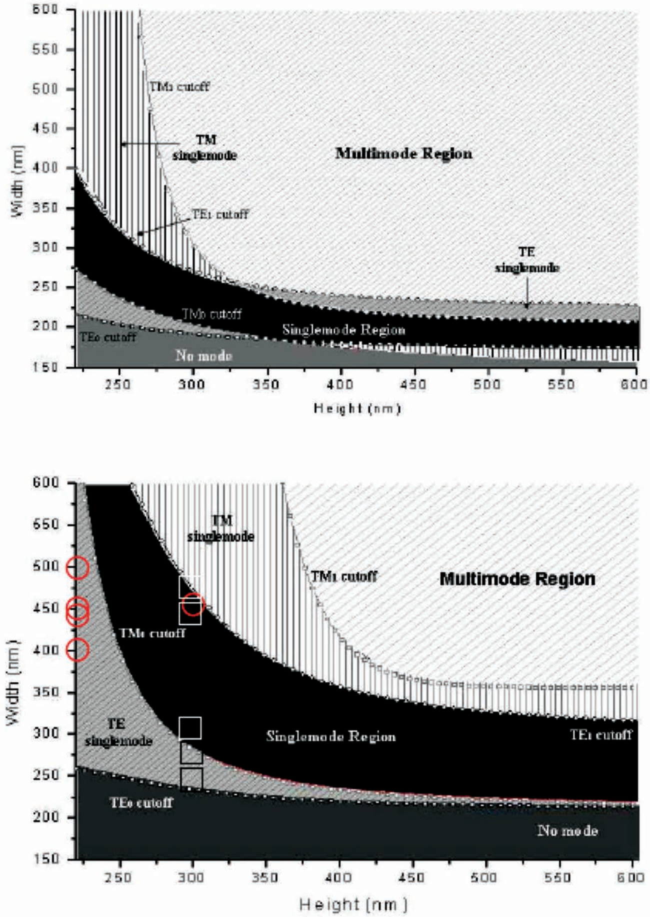

Figure 3.6 The single-mode condition for photonic wire at operation wavelengths of (a) 1330 nm and (b) 1550 nm. Reprinted with permission from Ref. [4] © The Optical Society.

For rib waveguides, in the middle of the cross section, there is a raised ridge region as the guided region that is similar to strip waveguides. But on both sides of the ridge the film is not completely removed, which is different to strip waveguides. The cross section of a rib waveguide in SOI is shown in Fig. 3.7. Due to the existence of the outside slab region, rib waveguides have a more complex mode characteristic, where high-order modes (modes other than the fundamental mode) can leak out from the slab region. Therefore, large rib waveguides even with micron-sized cross-sectional dimensions can behave as single-mode waveguides. However, strip waveguides support multiple modes when the cross-section dimensions reach a few hundred nanometers. Large rib waveguides, whose dimensions are closer to those of optical single-mode fibers, can achieve low-loss coupling to optical fibers. Rib waveguides have stronger confinement for light waves than strip waveguides, and we can fabricate electrodes on their slab region easily. So, the rib structure has been widely used for photonic waveguides.

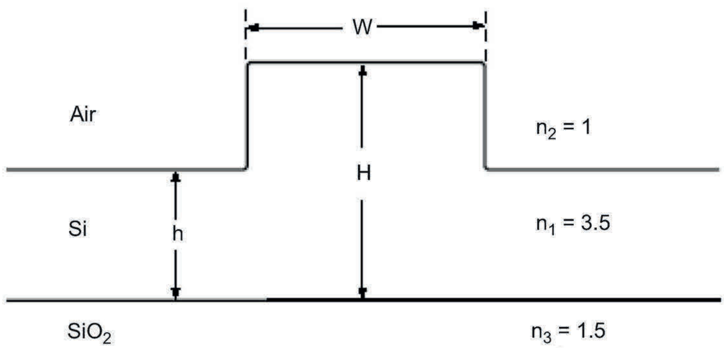

Figure 3.7 Cross section of a rib waveguide.

Petermann first proposed multimode rib waveguides with a large cross section [5]. Soref et al. used mode matching and BPMs to analyze the single-mode operation condition of optical GeSi-Si and Si-SiO_2 rib waveguides. They gave the following relation for single-mode conditions [6]:

$$\begin{cases} \dfrac{W}{H} \le 0.3 + \dfrac{r}{\sqrt{1-r^2}} \\ r = \dfrac{h}{H} \ge 0.5 \end{cases}, \tag{3.29}$$

where W is the rib width, H is the overall rib height, and h is the slab height, as shown in Fig. 3.7; r is the ratio of slab height to rib height. The second equation in Eqs. 3.29 represents a rib waveguide that is shallow-etched to ensure single-mode characteristics in the vertical direction of the rib waveguide. If $r > 0.5$, the effective index (propagation constant) of high-order modes in the vertical direction of the ridge region is smaller than that of the fundamental mode in the slab region, which makes high-order modes leak out of the guided region, leaving only fundamental modes in the vertical direction of the ridge region. After r is determined, the ratio W/H is determined by the first equation in Eqs. 3.29, which ensures single-mode characteristics in the horizontal direction of the rib waveguide.

Later, Rickman et al. and Schmidchen et al. studied the single- and multimode conditions of SOI rib waveguides by using experimental methods [7, 8]. They found a considerable difference between Soref's formula and the experimental results. Soref's formula is more relaxed than experimental data. On the basis of the above differences, many researchers analyzed the single-mode condition of large rib waveguides further using different numerical methods. Pogossian et al. studied the single-mode condition of the rib waveguide by using the EIM and obtained the single-mode condition [9], which is in better agreement with Rickman's experimental data, as shown in Fig. 3.8. The single-mode condition can be written as:

$$\begin{cases} \dfrac{W}{H} \leq \dfrac{r}{\sqrt{1-r^2}} \\ r = \dfrac{h}{H} \geq 0.5 \end{cases}, \tag{3.30}$$

where the variable definitions are the same as in Eq. 3.29.

Moreover, Xia et al. [10] analyzed the mode characteristics for rib waveguides with a trapezoidal cross section by using the BPM and then they obtained the single-mode condition for rib waveguides that is similar to Soref's formula.

The difference between numerical modeling and experiment may partly be explained by the different length scales. Theory considers stable modes in an infinite long waveguide, but in experiment light is coupled in and out after finite lengths.

When light waves couple with the waveguide from optical fibers, multiple different modes are exited in the waveguide due to discontinuous medium interfaces. Some modes constitute the guided modes in the waveguide, while the modes that cannot be guided in the waveguide leak out of the waveguide after a certain length [11]. The final stable field distribution in the waveguide is the superposition of the guided modes. It is possible to detect the high-order modes if the waveguide length is not long enough in the experiment and then to consider the waveguide as a multimode waveguide.

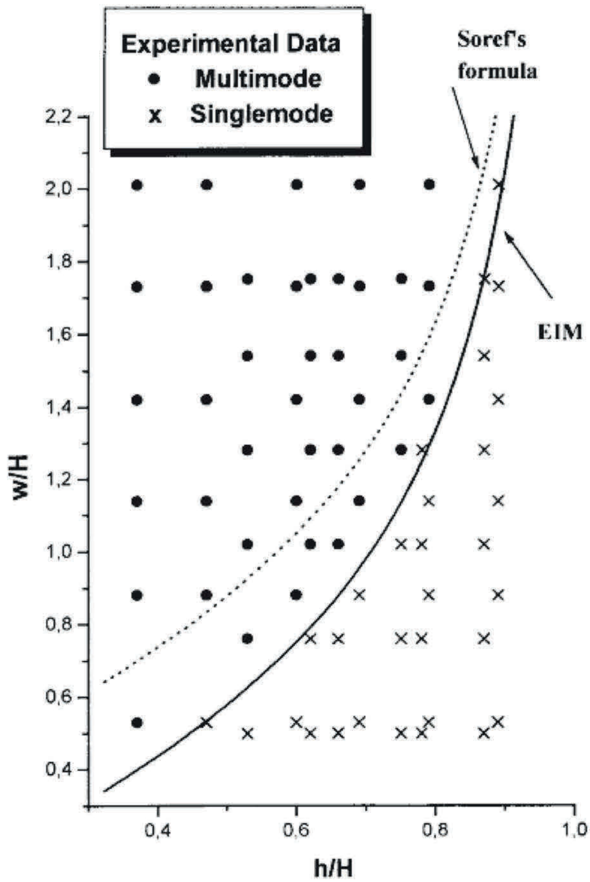

Figure 3.8 Different single-mode calculations of rib waveguides (Soref's formula, EIM) from Refs. [6, 9] compared to experimental data [7, 8] on a w/H versus h/H presentation.

However, the current trend is miniaturization and integration in silicon photonic devices to improve device performance and cost efficiency. When the cross-section dimensions of the rib waveguide reduce to around 1 μm or even to submicron levels, its single-mode condition is different to that of the large rib waveguide. The Yu [12] research group calculated the single-mode cutoff dimensions for quasi-TE and quasi-TM modes by using scalar and full-vector numerical simulation methods, respectively. It has been pointed out that small and deeply etched rib waveguides can satisfy the single-mode condition as long as the waveguide dimensions are designed reasonably. From the simulation data obtained, they give a fitting formula for the single-mode condition of small and deeply etched rib waveguides as follows:

$$\begin{cases} \dfrac{W}{H} \leq 0.05 + \dfrac{(0.94+0.25H)r}{\sqrt{1-r^2}} \\ 0.3 < r < 0.5, 1.0 \leq H \leq 1.5 \end{cases}, \tag{3.31}$$

where r is in the range of 0.3 to 0.5 because of polarization dependence.

Compared with the single-mode conditions given by Soref et al. and Pogossian et al., the simulation results of the single-mode condition for small-cross-section rib waveguides have the following characteristics.

- The ratio of slab height to rib height r is no longer limited to the condition $r > 0.5$. When the rib waveguide is deeply etched with $r < 0.5$, it can achieve single-mode transmission in the waveguide by choosing an appropriate waveguide width W.
- There is an obvious difference between the single-mode conditions for quasi-TE and quasi-TM modes, and the single-mode condition for the quasi-TM mode is more rigorous. Therefore, the single-mode condition for the quasi-TM mode should be the limiting condition for the waveguide design, because only when this is satisfied, both polarizations are single-mode ones.

3.3 Loss in a Silicon Optical Waveguide

With the development of the silicon micronanofabrication technology, single-mode propagation loss in a silicon waveguide has reduced to several decibels per centimeter from the initial several hundred decibels per centimeter. Low propagation losses of 0.8 dB/cm have been reported [13].

Loss reduction in the waveguide is very important for the quality of guided wave transmission. There are three main reasons for loss in the waveguide: absorption, scattering, and radiation. The losses caused by the three effects in a silicon waveguide are dependent on the waveguide design and micronanofabrication technology. In this section, we will discuss loss mechanisms in SOI waveguides.

The silicon in the SOI guided layer is transparent at the communication band in the range of 1.3 μm to 1.55 μm, so the loss of the SOI waveguide caused by intrinsic absorption is negligible. However, for some active photonic devices, free carriers are injected into the silicon by applying an external bias, which leads to free carrier absorption. The loss caused by free carrier absorption may be significant in the SOI waveguide. The absorption loss is proportional to the concentration of free carriers.

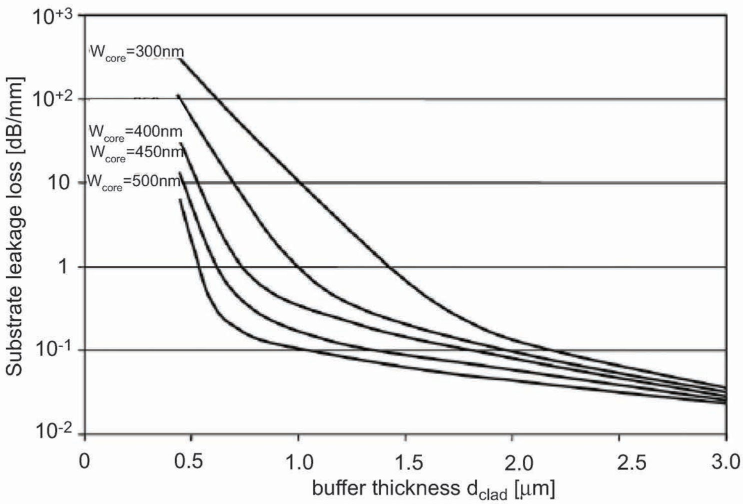

Figure 3.9 Substrate leakage loss of a photonic wire versus oxide thickness (parameter width *w*).

Substrate leakage is another important reason for propagation loss. In the case of submicron SOI waveguides, although they have strong confinement for light waves, a relatively large part of the mode field will leak into the cladding or substrate layer due to the small cross section. If the lower cladding layer of silica is too thin, the mode field even penetrates the buried oxide layer and couples with the silicon substrate, which leads to radiation loss. This leakage is larger due to smaller waveguide dimensions and a thinner buried oxide layer. Figure 3.9 shows the relationship between the loss of the TE mode in the waveguide with height H = 0.22 μm and the different widths caused by substrate leakage and the buried oxide thickness. It is clearly seen that the loss caused by substrate leakage decreases while the buried oxide thickness and waveguide width increase. Therefore, the buried oxide should be thick enough to reduce the substrate leakage loss.

For submicron waveguides, scattering caused by imperfections in the bulk waveguide material and roughness at the interface between different mediums in the waveguide is the main loss mechanism. The waveguide sidewalls are produced through lithography and etching process, so they are much rougher than the upper and lower interfaces of the silicon layer; and with the waveguide size shrinking further, the interaction between the mode field and rough sidewalls will be further enhanced, which leads to a sharp increase in the loss.

Sidewall roughness in the waveguide can change the waveguide width with random fluctuations, that is, the waveguide width is a random varying function along the propagation direction. Usually, we can use the standard deviation σ and the correlation length L_c to make a quantitative description for this function. These parameters can be measured through a variety of electron microscope experiments. Payne–Lacey theory indicates the scattering loss coefficient α (dB/cm) caused by the sidewall roughness in the waveguide as [14]:

$$\alpha = 4.34\frac{\sigma^2}{k_0\sqrt{2}w^4 n_{\mathrm{clad}}} g(V)\cdot f_{\mathrm{e}}(x,\gamma), \tag{3.32}$$

where $g(V)=\dfrac{U^2V^2}{1+W}$ is a function depending only on the waveguide geometry with the normalized coefficients $U = k_0 d\sqrt{n_{\mathrm{c}}^2 - n_{\mathrm{eff}}^2}$, $V = k_0 d\sqrt{n_{\mathrm{core}}^2 - n_{\mathrm{clad}}^2}$, and $W = k_0 d\sqrt{n_{\mathrm{eff}}^2 - n_{\mathrm{clad}}^2}$. The function f_{e} (x, γ) is linked to the sidewall roughness

$$f_e(x,\gamma) = \frac{x\sqrt{1-x^2+\sqrt{(1+x^2)^2+2x^2\gamma^2}}}{\sqrt{(1+x^2)^2+2x^2\gamma^2}}$$

$$x = W\frac{L_c}{d},\ \gamma = \frac{n_{cl}V}{n_c W\sqrt{\Delta}}$$

$$\Delta = \frac{n_{\text{core}}^2 - n_{\text{clad}}^2}{2n_{\text{core}}^2}, \tag{3.33}$$

where n_{core} and n_{clad} are the refractive indices of the core layer and the cladding layer, respectively; n_{eff} is the effective refractive index, w is the waveguide width, and k_0 is the free space wave number. Figure 3.10 shows the contour lines of the sidewall scattering loss versus the standard deviation σ and the correlation length L_c in the strip waveguide with a 200 nm × 200 nm cross-sectional dimension. The functions of $g(V)$ and $f_e(x, \gamma)$ in Eq. 3.32 are slowly varying functions depending on the waveguide parameters, which have little effect on waveguide loss, while the waveguide width and the standard deviation are the main factors for the waveguide loss.

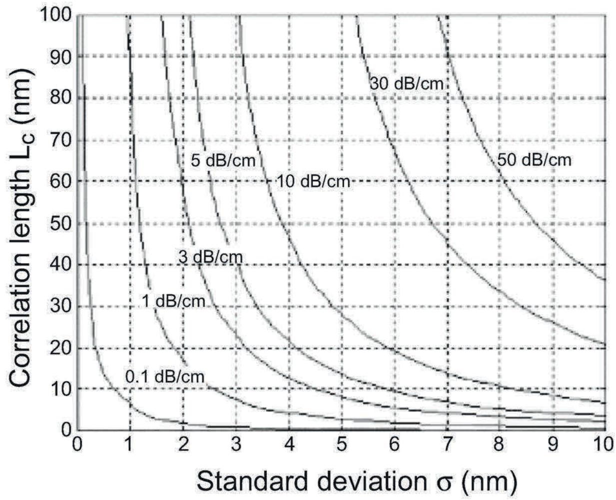

Figure 3.10 Contour lines of the sidewall scattering loss of a 200 nm × 200 nm strip waveguide as a function of (σ, L_c).

Measuring the loss in the waveguide is very important for designing photonic devices because the loss determines the quality of guided wave transmission in the waveguide. The propagation losses in the SOI single-mode strip waveguides have been measured by many research groups. There are many experimental methods associated with waveguide measurement, such as the cutback method, the Fabry–Perot resonance method, and the Fourier spectral analysis method. Table 3.1 shows some reported results.

Table 3.1 Comparison of the propagation loss measurement results for SOI single-mode strip waveguides (TE)

Reference	Height (nm)	Width (nm)	Propagation loss (dB/cm)	Wave length (nm)	Measurement method	Note
Sakai et al. [16]	320	400	25 ± 10	1550	Fabry–Perot	0.18 mm long
Lee et al. [13]	200	500	32 (traditional method) 0.8 (oxidation smoothing)	1540	Cutback	SiO_2 cladding
Almeida et al. [17]	270	470	5 ± 2	1550	Fabry–Perot	13 mm long
McNab et al. [18]	220	465	3.5 ± 2	1500	IR capture	4 mm long
Yamada et al. [19]	300	300	6	1550	Cutback	Oxidation smoothing, 16 mm long
		400	33.8 ± 1.7			
Dumon et al. [14]	220	450	7.4 ± 0.9	1550	Fabry–Perot	1 mm long
		500	2.4 ± 1.6			
Vlasov et al. [20]	220	445	3.6 ± 0.1	1500	Cutback	21 mm long

Bending of a waveguide leads to radiation losses in the bend. The magnitude of the bend loss strongly depends on the bend radius: the bend loss has a sharp increase with the radius curvature. It has been demonstrated in both theory and experiments that the bend loss in the submicron SOI strip waveguide is usually of the order of 0.1 dB, even with the bend radius R = 1 μm. Table 3.2 shows some bend loss measurement results of the single-mode SOI strip waveguides given in literature. To reduce the bend loss further, there are some methods: compact resonator structures are introduced into the bend to increase the transmissivity; the lateral offset is introduced into the junction between the straight waveguide and the bent waveguide to achieve better mode field matching.

Table 3.2 Comparison of bend loss measurement results for SOI single-mode strip waveguides (TE)

Reference	Height (nm)	Width (nm)	Radius (μm)	Loss (dB)	Wavelength (nm)
Lim [21]	200	500	1	0.5	1540
Sakai et al. [16]	320	400	1	1 ± 3	1550
Tsuchizawa et al. [22]	300	300	2	0.46	1550
			3	0.17	
Ahmad et al. [23]	340	400	Corner mirror	1	1550
Dumon et al. [24]	220	400	15	0.5	1550
			Corner mirror	1	
Vlasov et al. [20]	220	445	1	0.086 ± 0.005	1500
			2	0.013 ± 0.005	
			5	±0.005	

It is easier to obtain a small propagation loss in the rib waveguide because the side area is reduced. The propagation loss of a shallow-etched rib waveguide with ridge height H = 0.34 μm, width W = 0.50 μm, and slab height h = 0.14 μm is about 0.7 dB/cm [25]. However, the shallow-etched rib waveguide has weaker confinement in the lateral direction, so light in the ridge waveguide leaks out easily from the slab region. Usually, the ridge waveguide requires a longer bend radius to obtain a low bend loss. Therefore, the rib waveguides often use corner reflectors to achieve a 90º deflection of rays. The bend loss in the rib waveguide with corner reflectors was reduced to 0.32 ± 0.02 dB (92.9% bend efficiency) for TE polarization at $\lambda = 1.55$ μm [26].

3.4 Polarization Dependence of Silicon Waveguides

Polarization dependence in SOI optical waveguides of small dimensions is rather strong. As already shown in Fig. 3.2, there is a difference between the TE and TM field strength distributions in the waveguide. Figure 3.11 shows the field distributions and loss spectra for TE and TM modes in a single-mode SOI strip waveguide.

Usually, polarization dependence is described by waveguide birefringence, which is defined as the effective index or group refractive index difference between TE and TM modes,

$$\Delta n_{\text{eff}} = n_{\text{eff}}^{\text{TE}} - n_{\text{eff}}^{\text{TM}}.$$

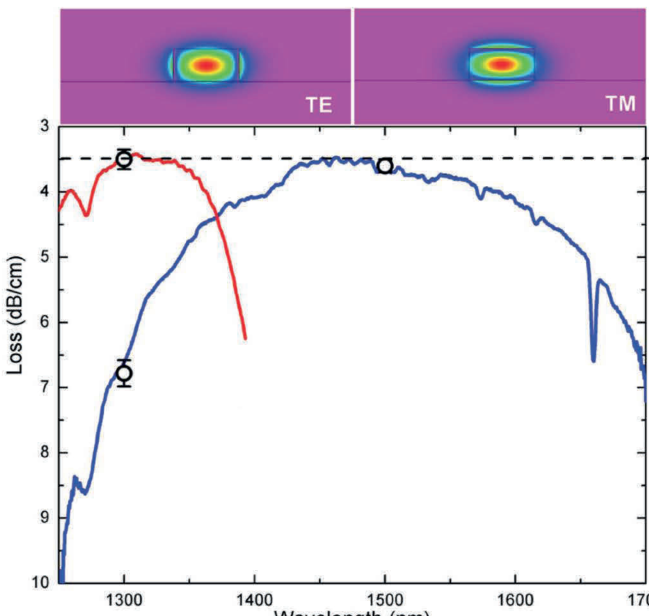

Figure 3.11 The mode field distributions (above) and loss spectra (below) for TE and TM modes in a single-mode SOI strip waveguide.

Figure 3.12 shows the relationship between the effect refractive index and the waveguide width, where four colored lines represent TE and TM modes in the strip and rib waveguides, respectively. The effective refractive index for the TE mode can be equal to the one for the TM mode in the waveguide at some specific dimensions in order to achieve zero birefringence. However, it should be noted that a deviation in the waveguide width will cause a change in the birefringence. When the strip waveguide width has a 10 nm deviation, the birefringence deviation reaches the order of 10^{-2}.

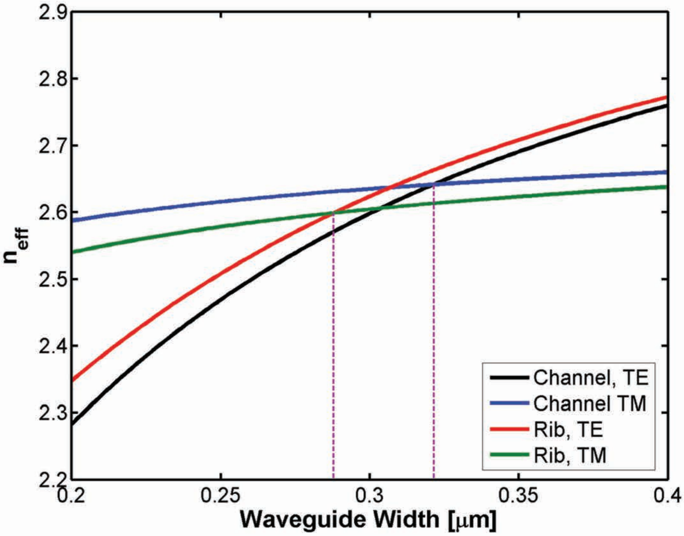

Figure 3.12 Effective refractive index of TE and TM modes in the strip and rib waveguides.

Birefringence control from the geometry and dimension of the waveguide requires precise dimension control with a high requirement for fabrication tolerance. The waveguide birefringence of a given waveguide may be changed by two mechanisms: asymmetry of the structure and the opto-elastic effect due to anisotropic stress in the waveguide core layer. Therefore, we could consider these two aspects to reduce polarization dependence.

A silica cladding usually covers the silicon core layer of SOI waveguides. The stress in the upper cladding layer causes anisotropic stress distribution in the core and at the edge of the silicon layer, and the refractive indices of silicon and silica are changed by the elastic-optic effect; a stress-related birefringence component is introduced. The birefringence caused by stress is related to the oxide density, oxide thickness, and waveguide geometric. Therefore, the waveguide birefringence can be effectively reduced by properly changing the upper cladding thickness and the stress in the material.

3.5 Summary

Silicon has shown great advantage for photonic waveguiding, especially for optoelectronic integration. SOI has become the most popular platform for silicon photonic waveguides due to the high refractive index contrast between the semiconductor and the surrounding silicon oxide. To discuss basic waveguide properties, we began with Maxwell's equations, analyzed the mode field distributions in the slab waveguide, extended that to the strip and rib waveguides, and then gave a comprehensive analysis of single-mode conditions for the waveguides. Basic loss mechanisms and polarization properties were discussed, with reference to experimental results and numerical calculations. Nanowire waveguides are the backbone of chip-sized photonic systems; they transport optical signals between sources and receivers, splitters divide the signal into various directions, and different signals are added at waveguide combiners. The high refractive index contrast of SOI waveguides allows dense packing of many waveguides, with strong bending on a silicon chip.

Acknowledgements

We thank Xuejun Xu and Kang Xiong for collection of basic informations and figure drawings.

References

1. M. Born and E. Wolf (1999). *Principles of Optics* (Cambridge Univ. Press, Cambridge, UK).
2. W. Bogaerts, D. Taillaert, B. Luyssaert, P. Dumon, J. Van Campenhout, P. Bienstman, D. Van Thourhout, R. Baets, V. Wiaux and S. Beckx (2004).

Basic structures for photonic integrated circuits in silicon-on-insulator, *Opt. Express*, **12**, 1583–1591.

3. D. Dai, Y. Shi and S. He (2006). Characteristic analysis of nano silicon rectangular waveguides for planar light-wave circuits of high integration, *Appl. Opt.*, **45**, 4941–4946.
4. S. T. Lim, C. E. Png, E. A. Ong and Y. L. Ang (2007). Single mode, polarization-independent submicron silicon waveguides based on geometrical adjustments, *Opt. Express*, **15**, 11061–11072.
5. K. Petermann (1976). Properties of optical rib-guides with large cross-section, *Archiv für Elektronik und Überetragungstechnik*, **30**, 139–140.
6. R. A. Soref, J. Schmidtchen and K. Petermann (1991). Large single-mode rib waveguides in GeSi-Si and Si-on-SiO_2, *IEEE J. Quantum Electron.*, **27**, 1971–1974.
7. A. G. Richman, G. T. Reed and F. Namavar (1994). Silicon-on-insulator optical rib waveguide loss and mode characteristics, *J. Lightwave Technol.*, **12**, 1771–1776.
8. J. Schmidtchen, A. Splett, B. Schuppert, K. Petermann and G. Burbach (1991). Low loss singlemode optical waveguides with large cross-section in silicon-on-insulator, *Electron. Lett.*, **27**, 1486.
9. S. P. Pogossian, L. Vescan and A. Vonsovici (1998). The single-mode condition for semiconductor rib waveguides with large cross section, *J. Lightwave Technol.*, **16**, 1851–1853.
10. J. Xia and J. Yu (2004). Single-mode condition for silicon rib waveguides with trapezoidal cross-section, *Opt. Commun.*, **230**, 253–257.
11. J. Lousteau, D. Furniss, A. B. Seddon, T. M. Benson, A. Vukovic and P. Sewell (2004). The single-mode condition for silicon-on-insulator optical rib waveguides with large cross section, *J. Lightwave Technol.*, **22**, 1923–1929.
12. X. Xu, S. Chen, J. Yu and X. Tu (2009). An investigation of the mode characteristics of SOI submicron rib waveguides using the film mode matching method, *J. Opt. A: Pure Appl. Opt.*, **11**, 015508.
13. K. K. Lee, D. R. Lim, L. C. Kimerling, J. Shin and F. Cerrina (2001). Fabrication of ultralow-loss Si/SiO2 waveguides by roughness reduction, *Optics Lett.*, **26**, 1888–1890.
14. P. Dumon, W. Bogaerts, V. Wiaux, J. Wouters, S. Beckx, J. Van Campenhout, D. Taillaert, B. Luyssaert, P. Bienstman, D. Van Thourhout and R. Baets (2004). Low-loss SOI photonic wires and ring resonators fabricated with deep UV lithography, *IEEE Photonics Technol. Lett.*, **16**, 1328–1330.

15. F. Grillot, L. Vivien, S. Laval, D. Pascal and E. Cassan (2004). Size influence on the propagation loss induced by sidewall roughness in ultrasmall SOI waveguides, *IEEE Photonics Technol. Lett.*, **16**, 1661–1663.
16. A. Sakai, G. Hara and T. Baba (2001). Propagation characteristics of ultrahigh-Δ optical waveguide on silicon-on-insulator substrate, *Jpn. J. Appl. Phys.*, **40**, L383–L385.
17. V. R. Almeida, R. R. Panepucci and M. Lipson (2003). Nanotaper for compact mode conversion, *Opt. Lett.*, **28**, 1302–1304.
18. S. J. McNab, et al. (2003). Ultra-low loss photonic integrated circuit with membrane-type photonic crystal waveguides, *Opt. Express*, **11**, 2927–2939.
19. K. Yamada, et al. (2004). Microphotonics devices based on silicon wire waveguiding system, *IEICE Trans. Electron.*, **E87-C**(3), 351–358.
20. Y. A. Vlasov, et al. (2004). Losses in single-mode silicon-on-insulator strip waveguides and bends, *Opt. Express*, **12**, 1622–1631.
21. D. R. Lim (2000). Device integration for silicon microphotonics platforms, PhD thesis, MIT.
22. T. Tsuchizawa, T. Watanabe, E. Tamechika, T. Shoji, K. Yamada, J. Takahashi, S. Uchiyama, S. Itabashi and H. Morita (2002). Fabrication and evaluation of submicron-square Si wire waveguides with spot-size converters, *Paper TuU2 presented at LEOS Annual Meeting*, Glasgow, UK, p. 287.
23. R. U. Ahmad, F. Pizzuto, G. S. Camarda, R. L. Espinola, H. Rao and R. M. Osgood, Jr. (2002). Ultracompact corner-mirrors and T-branches in silicon-on-insulator, *IEEE Photonics Technol. Lett.*, **14**, 65.
24. P. Dumon, W. Bogaerts, J. Van Campenhout, V. Wiaux, J. Wouters, S. Beckx and R. Baets (2003). Low-loss photonic wires and compact ring resonators in silicon-on-insulator, *LEOS Benelux Annual Symposium 2003*, Netherlands.
25. M. A. Webster, R. M. Pafchek, G. Sukumaran and T. L. Koch (2005). Low-loss quasi-planar ridge waveguides formed on thin silicon-on-insulator, *Appl. Phys. Lett.*, **87**, 231108-1-3.
26. Y. Qian, S. Kim, J. Song, G. P. Nordin and J. Jiang (2006). Compact and low loss silicon-on-insulator rib waveguide 90° bend, *Opt. Express*, **14**, 6020–6028.